Triosephosphate isomerase from *Plasmodium falciparum*: the crystal structure provides insights into antimalarial drug design

Sameer S Velanker[1], Soumya S Ray[1], Rajesh S Gokhale[1], Suma S[1], Hemalatha Balaram[2], P Balaram[1] and MRN Murthy[1]*

Background: Malaria caused by the parasite *Plasmodium falciparum* is a major public health concern. The parasite lacks a functional tricarboxylic acid cycle, making glycolysis its sole energy source. Although parasite enzymes have been considered as potential antimalarial drug targets, little is known about their structural biology. Here we report the crystal structure of triosephosphate isomerase (TIM) from *P. falciparum* at 2.2 Å resolution.

Results: The crystal structure of *P. falciparum* TIM (PfTIM), expressed in *Escherichia coli*, was determined by the molecular replacement method using the structure of trypanosomal TIM as the starting model. Comparison of the PfTIM structure with other TIM structures, particularly human TIM, revealed several differences. In most TIMs the residue at position 183 is a glutamate but in PfTIM it is a leucine. This leucine residue is completely exposed and together with the surrounding positively charged patch, may be responsible for binding TIM to the erythrocyte membrane. Another interesting feature is the occurrence of a cysteine residue at the dimer interface of PfTIM (Cys13), in contrast to human TIM where this residue is a methionine. Finally, residue 96 of human TIM (Ser96), which occurs near the active site, has been replaced by phenylalanine in PfTIM.

Conclusions: Although the human and *Plasmodium* enzymes share 42% amino acid sequence identity, several key differences suggest that PfTIM may turn out to be a potential drug target. We have identified a region which may be responsible for binding PfTIM to cytoskeletal elements or the band 3 protein of erythrocytes; attachment to the erythrocyte membrane may subsequently lead to the extracellular exposure of parts of the protein. This feature may be important in view of a recent report that patients suffering from *P. falciparum* malaria mount an antibody response to TIM leading to prolonged hemolysis. A second approach to drug design may be provided by the mutation of the largely conserved residue (Ser96) to phenylalanine in PfTIM. This difference may be of importance in designing specific active-site inhibitors against the enzyme. Finally, specific inhibition of PfTIM subunit assembly might be possible by targeting Cys13 at the dimer interface. The crystal structure of PfTIM provides a framework for new therapeutic leads.

Addresses: [1]Molecular Biophysics Unit, Indian Institute of Science, Bangalore-560012, India and [2]Jawaharlal Nehru Center for Advanced Scientific Research, Jakkur, Bangalore-560064, India.

*Corresponding author.
E-mail: mrn@mbu.iisc.ernet.in

Key words: β barrel, drug design, malaria, *Plasmodium falciparum*, triosephosphate isomerase

Introduction

Plasmodium falciparum is the most prevalent species of malarial parasite in the Asian subtropical zone. The parasite is responsible for malignant subtertian malaria. Globally, more than 120 million clinical cases and over one million deaths occur due to malaria every year. Control of this disease has been a major focus of attention of the World Health Organization.

The parasite lacks a functional tricarboxylic acid cycle [1]. The asexual stage of the parasite, residing in the mature human erythrocyte, solely depends on glycolysis for its ATP requirements. The glucose consumption of the infected erythrocytes increases by 50–100 fold over that of uninfected erythrocytes. In infected erythrocytes, the flux of several glycolytic enzymes are elevated [2]. Glycolytic enzymes are believed to associate with membrane components facilitating channeling of the substrate between consecutive glycolytic enzymes during triosephosphate metabolism [3]. Glycolysis in the parasite might be inhibited either by designing specific inhibitors for the enzymes of the pathway or by disrupting the microassembly on the cytoskeleton. Three-dimensional structures of glycolytic enzymes of

P. falciparum will be of undoubted value in designing new strategies for therapeutic intervention.

Triosephosphate isomerase (TIM) is a dimeric glycolytic enzyme, which catalyzes the isomerization of D-glyceraldehyde-3-phosphate to dihydroxyacetone phosphate. Extensive mutagenesis experiments on the yeast protein suggest that TIM is an 'evolutionarily perfect enzyme' (i.e. any mutations in the enzyme reduce efficiency/stability) [4]. TIM also plays an important role in gluconeogenesis, the hexosemonophosphate shunt and fatty acid biosynthesis. Crystal structures for the enzyme have been determined from several sources. There has been a recent report that during malarial infection, patients mount an antibody response to TIM resulting in prolonged hemolytic anemia [5]. This raises the possibility that the protein may become localized on the erythrocyte membrane, becoming partly exposed. Indeed TIM from the parasite *Schistosoma mansoni* was shown to be a surface antigen and has been considered for vaccine development [6].

Seven of the eleven glycolytic enzymes from *P. falciparum* have been cloned and sequenced (Table 1). We previously reported the cloning and overexpression of *P. falciparum* TIM (PfTIM) [7]. Relatively little is known about the structural biochemistry of parasite glycolytic enzymes, although these have been considered as potential targets for antimalarial drug development [8]. Indeed at the present time only one three-dimensional structure has been reported for a glycolytic enzyme from *P. falciparum* [9]. In this paper we report the crystal structure of PfTIM determined at 2.2 Å resolution.

The PfTIM structure has the overall α/β-barrel fold, as observed in other TIM structures [10]. However, comparison of PfTIM with human TIM reveals several important differences. Most significantly a strongly conserved surface residue (Glu183) is replaced by a hydrophobic residue (Leu183) in the parasite enzyme. Two other important differences include a cysteine residue (Cys13) located in the dimer interface instead of the methionine residue found in human TIM and the replacement of a conserved Ser96 residue in the active site by Phe96 in the parasite protein.

Results and discussion

PfTIM structure determination

The structure of PfTIM was determined using the trypanosomal TIM as the starting model. Despite the 58% amino acid sequence difference between the two proteins, the trypanosomal structure was found to be an excellent starting model. Both rotation and translation function [11] solutions leading to placement of the trypanosomal enzyme in the PfTIM unit cell were unambiguous. Initial, rigid-body refinement of the two monomers of the dimeric enzyme led to only small changes in the relative orientation and position, suggesting that the quaternary structures of the two enzymes are very similar. The $2F_o–F_c$ map computed after rigid-body refinement could be interpreted easily in terms of the PfTIM sequence. The first two N-terminal residues in both of the monomers did not have significant density in the initial map. Starting from this initial model, the final structure was obtained by the refinement protocol described in the Materials and methods section. A total of 171 water molecules could be located in difference Fourier maps and were found to have temperature factors of less than 50 $Å^2$ during subsequent refinement. The Cα trace of the dimeric structure of PfTIM is illustrated in Figure 1.

Final electron-density map

The quality of the final $2F_o–F_c$ electron-density map is shown in Figure 2. The course of the polypeptide mainchain in both of the monomers (A and B) was unambiguous. In the structure of other TIMs, a large degree of mobility is observed for the loop consisting of residues 168–180 (loop 6; trypanosomal TIM nomenclature) [12,13]; these residues are known to be proximal to the active site. The sidechains of all the residues of this loop had well defined density in both subunits in the PfTIM structure. The residues Lys12, His95 and Glu165, which

Table 1

Glycolytic enzymes cloned from *Plasmodium falciparum*.

Enzyme	Sequence	Reference	Crystal structure	Reference
Hexokinase	Known	[46]	Not known	
Glucose phosphate isomerase	Known	[47]	Not known	
Phosphofructokinase	Not known		Not known	
Aldolase	Known	[27]	Not known	
Triosephosphate isomerase	Known	[7]	Known	This paper
Glyceraldehyde-3-phosphate dehydrogenase	Not known		Not known	
3-Phosphoglycerate kinase	Known	[48]	Not known	
Phosphoglyceromutase	Not known		Not known	
Enolase	Known	[49]	Not known	
Pyruvate kinase	Not known		Not known	
Lactate dehydrogenase	Known	[9] Unpublished data	Known	[9]

Figure 1

Stereoview Cα trace of the dimer of PfTIM. The view is along the β-barrel axis of one of the monomers. This figure clearly shows that the β-barrel axes are not parallel to the twofold axis relating the two monomers.

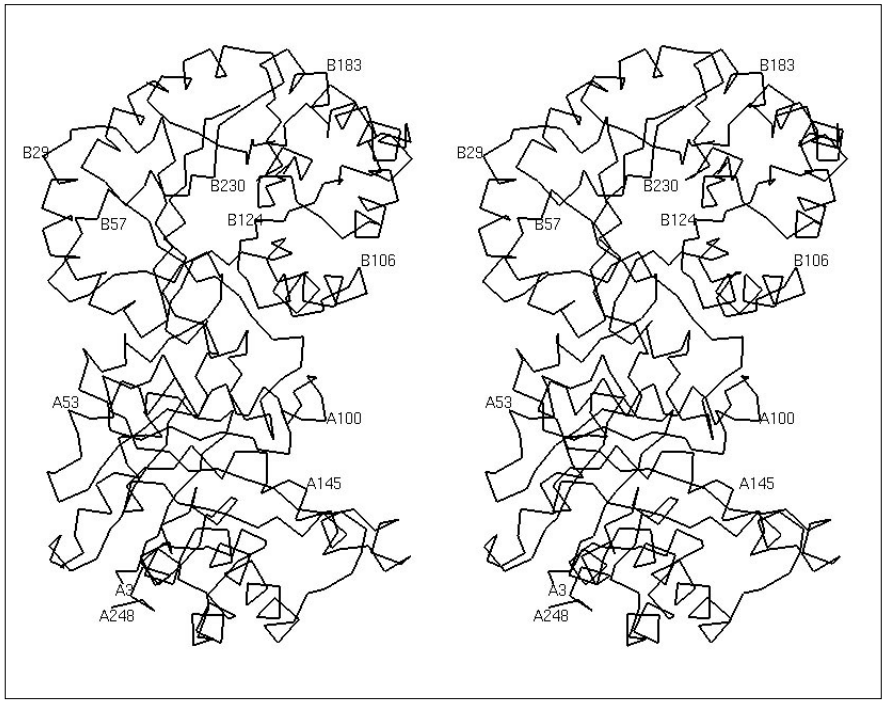

are known to be part of the TIM active site, are found to be ordered in the PfTIM structure. The electron-density map is consistent with the amino acid sequence deduced from the corresponding gene sequence [7] at all positions except one, residue 163. Here, both F_o–F_c and $2F_o$–F_c maps clearly suggest a residue with a branched sidechain, in contrast to the alanine deduced from the gene sequence and found in all the known TIM sequences. This residue has been tentatively assumed to be a valine in the PfTIM structure (Fig. 3). This observation suggests that the Ala163→Val replacement in PfTIM may be a result of a translational error due to overexpression of the cloned gene. Such errors have been reported to occur in other overexpression systems [14].

The monomer fold

The polypeptide fold is a classical α/β-barrel structure. There are 8 β-strands which form the inner core of the barrel; the α helices form the outer layer of the structure. The active site of the protein is at the C-terminal end of the barrel, as found in all other α/β-barrel proteins. Following the nomenclature used for the description of

Figure 2

Stereoview of the $2F_o$–F_c electron-density map at 2.2 Å resolution for the region spanning residues in loop 6. The region around the active-site residue Glu165 is included in the map. (The picture was prepared using the program O [45].)

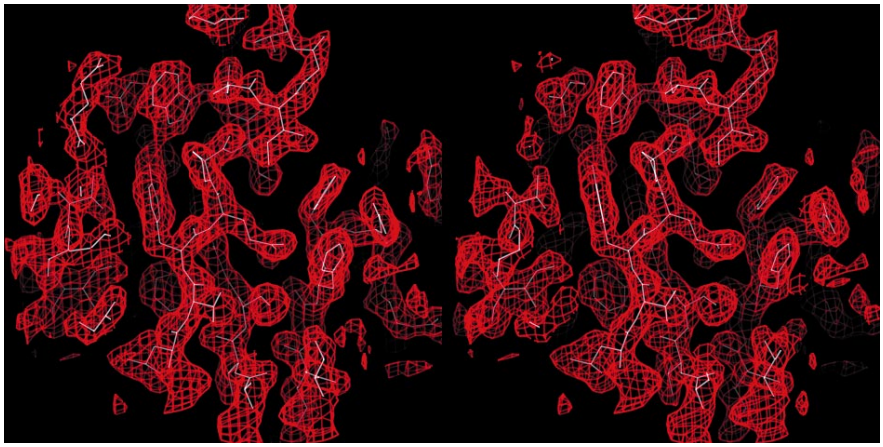

Figure 3

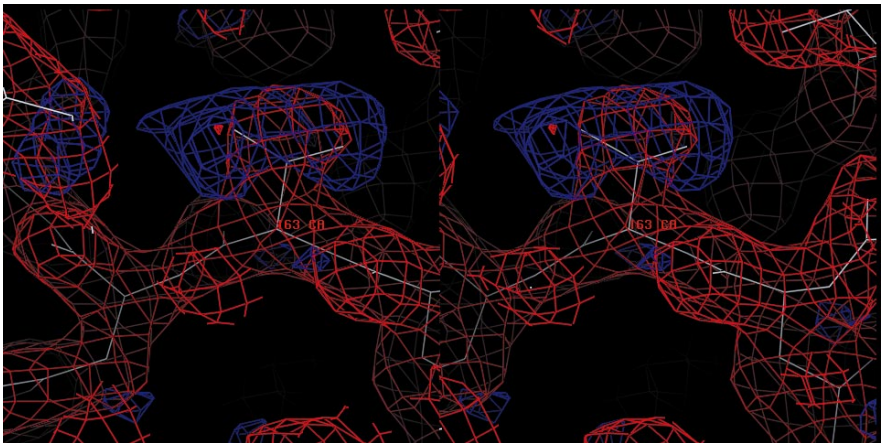

The $2F_o–F_c$ (red) and $F_o–F_c$ (blue) maps around residue 163. These maps clearly indicate that the residue at position 163 has a branched sidechain.

trypanosomal TIM structures [15], the strands, loops and the helices of the barrels are numbered 1–8 and the two monomers are designated as A and B.

Only two residues, the active site Lys12 from both monomers, lie within the less favorable, albeit generously allowed, regions of the Ramachandran plot [16] (ϕ=51.6°, ψ=–148.3° in the A subunit; ϕ= 53.5°, ψ= –144.2° in the B subunit). Such a deviation is also observed in the other TIM structures. The unfavorable conformation of Lys12 is stabilized by interactions with Asn10, Asn14 and Asn64. The only other residue that occurs in the generously allowed region of the Ramachandran plot is Asp152 in the B subunit (ϕ= –32.7°, ψ= 73.8°). Superposition of the two monomers of PfTIM leads to a root mean square (rms) deviation between the corresponding Cα atoms of 0.45 Å. There are no segments that are strikingly different between the two subunits. The segment with the maximum difference between the A and B subunits corresponds to the flexible loop 6 from the two subunits.

PfTIM has two tryptophan residues per monomer which are solvent inaccessible. One of the tryptophans is at the dimeric interface (Trp11), which serves as a good probe to monitor subunit dissociation during the course of unfolding. The other tryptophan is conserved in all the known TIM sequences and lies in the mobile loop 6 (Trp168). This second tryptophan serves as a probe to monitor the loop 6 environment during TIM catalysis. The observed fluorescence emission maximum of 331 nm for PfTIM is in agreement with the hydrophobic environment for the two tryptophan residues (RSG, SSR, HB and PB, unpublished data). The emission maximum of completely solvent exposed tryptophans is about 356 nm [17].

Figure 4 shows the variation of B factor along the polypeptide chain for the two monomers. Loop 6 has higher B factors in both the subunits, as observed in the other TIM structures [18,19]. In addition, loop 5 (which contains Asp152) and the C terminus of helix 5 have higher B factors in the B subunit, while a short peptide segment (between helix 5 and strand 6) has higher thermal parameters in the A subunit. The N and the C termini in both of the subunits display higher B factors. The χ^1 angles of most of the residues in the A subunit, with B factors less than 30 $Å^2$, are in good agreement with the corresponding values from the B subunit. The χ^1 angles appear to be genuinely different in the two subunits for only 12 residues (Asn25, Leu55, Lys58, Glu81, Arg110, Glu135, Thr139, Asp152, Asp155, Glu179, Ser218 and Ser219). Except for Leu55, all the other 11 residues are polar with hydrogen-bonding potential and are exposed on the surface of the dimer.

Geometry of the β barrel

Individual strands make an angle of 48–64° with the β-barrel axis. Consecutive strands of the barrel are at an angle of 12–57°. The helical axes are at angles of 130–144° to the barrel axis; the angle between a β strand and the associated helix axis varies between 136–171°. The core of the β barrel is packed with hydrophobic residues from the β strands (Phe6, Ala8, Val40, Phe42, Gly62, Tyr90, Ile92, Val124, Cys126, Ile161, Val163, Ile207, Gly228 and Leu230). Most of these core residues are conserved in human and trypanosomal TIM. However, Phe42 and Val163 of PfTIM are both replaced by alanine residues in the human [20] and trypanosomal enzymes. The total van der Waals volume of the residues of the barrel interior in the human and trypanosomal enzymes are comparable (~1372 $Å^3$), while that of PfTIM is larger (1471 $Å^3$). The difference (99 $Å^3$) corresponds to a volume larger than that occupied by a phenyl group. In addition, the mean hydrophobicity of the residues found in PfTIM is larger than the corresponding value in the human and trypanosomal enzymes. The amino acid replacements are consistent with the observed higher stability in urea denaturation

Figure 4

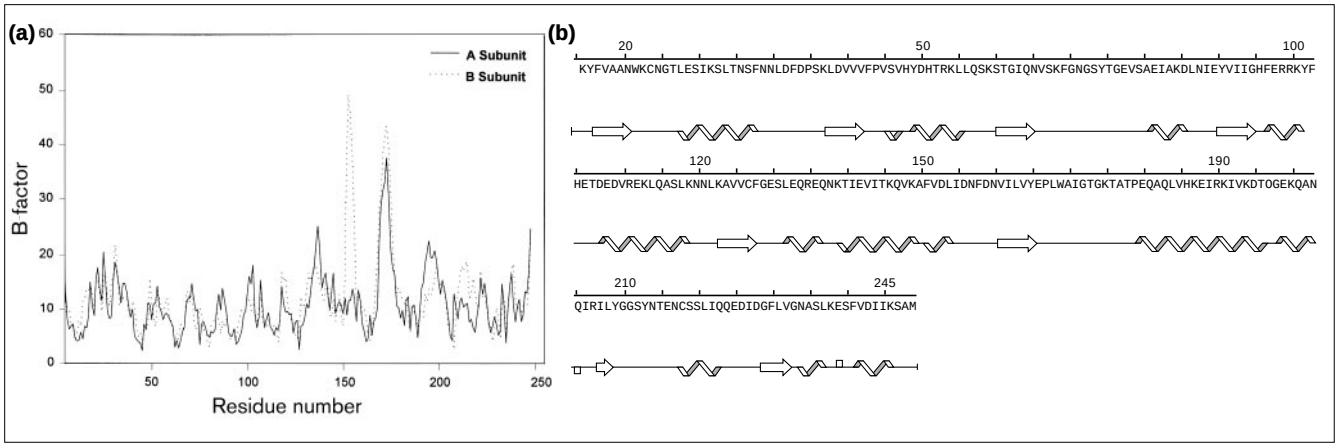

Variation of B factor along the polypeptide chain. The solid and dotted lines in (a) represent the A and B subunits of PfTIM, respectively. (b) The secondary structure elements along the polypeptide chain of PfTIM highlighting the correlation between the secondary structure elements and thermal factors. Arrows represent the β strands. (The figure was made using PROCHECK [50].)

experiments of PfTIM (RSG, SSR, HB and PB, unpublished data) when compared to the human enzyme [21].

Subunit association

The two subunits of PfTIM are related by a rotation of 178.6°. The overall surface area buried in the dimeric interface of PfTIM is 1800 Å^2 per subunit, which constitutes 15.5% of the total solvent accessible area of the isolated A and B monomers. The largest contribution to this buried area comes from loop 3 which intimately interacts with loop 1 of the other subunit. In the PfTIM dimer 12.4% (1478 Å^2) of the total polar surface (11 901 Å^2) and 19% (2163 Å^2) of the total nonpolar surface (11 361 Å^2) becomes solvent inaccessible upon dimerization. In human TIM [20] the total polar and nonpolar surface areas of the two isolated monomers are 9839 Å^2 and 11 992 Å^2, respectively. On dimerization, 16% of the polar (1615 Å^2) and 16.1% of the nonpolar (1935 Å^2) surface becomes buried. These observations suggest that the interface of human TIM is significantly more polar and might be weaker as compared to PfTIM.

Differences between the human and PfTIM structures

We present here a comparative analysis of PfTIM and human TIM, which might be of importance for understanding the function and stability of the enzymes and highlights the differences between them.

A superposition of the polypeptide fold of the A subunit of PfTIM with the corresponding subunits of human and trypanosomal TIM's is shown in Figure 5. Apart from loop 6, there are four regions (residues 18–31, 47–57, 68–78 and 141–153) with significant deviation in the corresponding Cα positions between human TIM and PfTIM. These differences are also observed in the superposition of the corresponding B subunits of the human and PfTIM's. These segments, except for helix 5 from the B subunit, are clustered in the intersubunit interface.

Residues 3–35 of PfTIM are structurally equivalent to 4–36 of the human enzyme. Residue 36 (lysine) is an insertion in the PfTIM with respect to the human enzyme. The rest of the residues 37–248 are structurally equivalent in the two enzymes. Only five residues, surrounding the lysine insertion site in PfTIM, show large deviations from the corresponding residues in human TIM. None of the residues of the loops at the N-terminal end of the β barrel are conserved between the two enzymes, while only two of the 85 (2.4%) residues constituting the helical segments are conserved. In contrast, ten of the 53 residues in the β strands (10.9%) and 23 of 64 residues (35.9%) of the loops at the C-terminal end of the barrel are conserved. The higher conservation observed in the loops at the C-terminal end of the barrel reflects the involvement of these loops in the function and integrity of the enzyme. Of the 14 residues lining the inner side of the β barrel, six are conserved.

The superposition of PfTIM and trypanosomal TIM reveals three segments, apart from the loop 6, which show significant structural deviations. These regions show a similar deviation in their Cα positions in the corresponding B subunits. The segments correspond to residues 50–59, 68–71 and 151–159. The first two of these segments correspond to the intersubunit interface, while residues 151–159 correspond to the N-terminus of β strand 6. As most of the regions which show significant deviations between the human and trypanosomal TIMs and PfTIM are in the

Figure 5

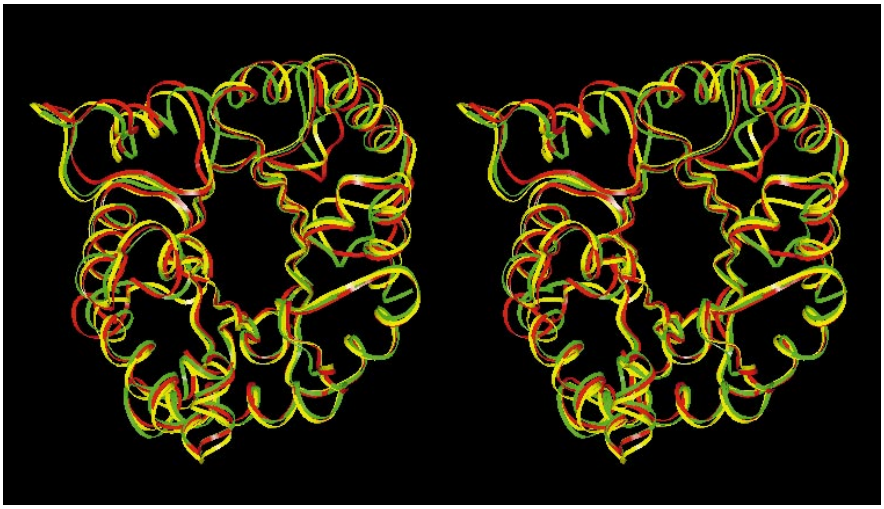

Stereoview superposition of the Cα atoms of monomer A of trypanosomal TIM, human TIM and PfTIM shown in red, green and yellow, respectively. (The figure was made using INSIGHT II [51].)

intersubunit interface, they are excluded from interactions resulting from crystal packing. Hence, these differences are likely to represent real differences in the geometry of the interface in these homologous enzymes.

The active site

Figure 6 illustrates the superposition of polypeptide segments from the PfTIM and human TIM structures, which include the active-site residues Lys12, His95 and Glu165. In accordance with earlier reports [22] the residues in the active site are not rigid, the most flexible being Glu165.

Residues 165–178 in PfTIM constitute the flexible loop 6 which is known to undergo a large movement upon ligand binding [13]. The sidechain of the active-site Glu165 has been observed to adopt two different conformations: a

Figure 6

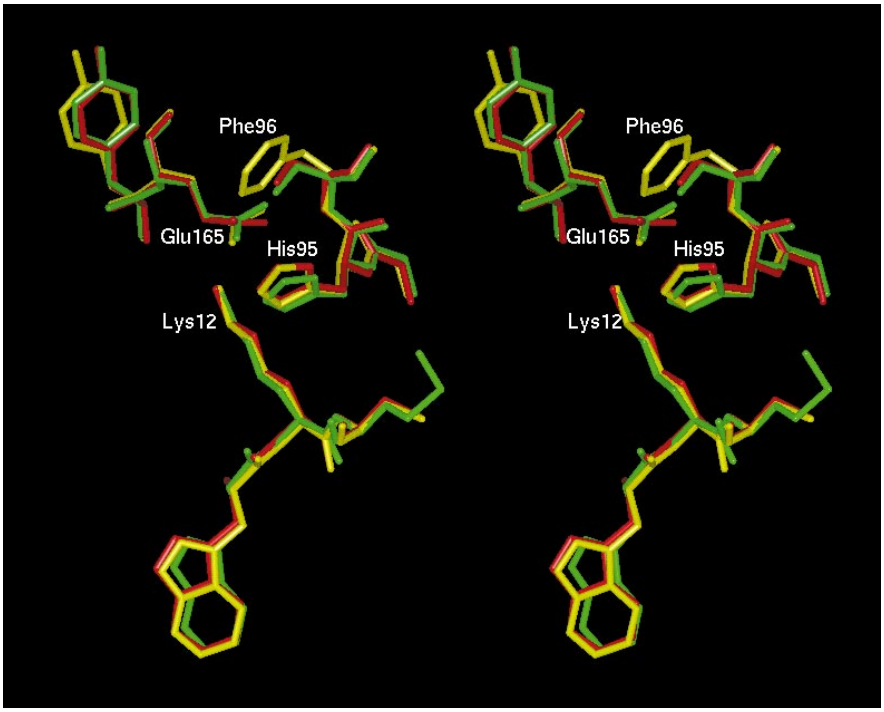

Superposition of the active-site residues from human TIM, trypanosomal TIM and PfTIM shown in red, green and yellow, respectively. The active-site residues, Glu165, His95 and Lys12, are labeled. Phe96 of PfTIM, which is a serine residue in the human and trypanosomal TIMs, is close to the active-site residues Glu165 and His95 and is also labeled.

'swung-in' position (with $\chi^1 = +60°$) that is suitable for catalysis [22] and a 'swung-out' position (with $\chi^1 = -60°$) which is observed in the ligand free state. The position of Glu165 observed in PfTIM corresponds to $\chi^1 = -58°$ and is not suitable for catalysis. This is consistent with the absence of a ligand bound at the active site. Accordingly, the active site superposes well with human and trypanosomal TIM A subunit (active site unoccupied; Fig. 6), while it shows a large deviation with respect to the trypanosomal TIM B subunit (active site occupied with a sulfate ion). More recent evidence from solid state NMR studies [23] suggest that loop 6 is inherently flexible and ligands have a pronounced effect on the loop structure. Verlinde *et al.* observed the active-site loop in an 'open' conformation even though the active site is occupied by a substrate analog in the crystal [24]. Loop 6 in PfTIM is in an open conformation and the associated segment has comparatively large thermal factors.

Residue 96 is a serine in most of the TIMs studied but is a phenylalanine residue in PfTIM. The serine residue in other TIMs forms hydrogen bonds with the catalytic residues His95 and Glu165. The specific activities of PfTIM (6880–7230 units mg^{-1}) and human TIM (9800 units mg^{-1}) are comparable, suggesting that the hydrogen bonds between residue 96 and the catalytic residues do not play an important role in catalysis.

Surface hydrophobic patch on PfTIM

Residue 183 is a leucine in PfTIM, but is replaced by a glutamate in human TIM. Surface accessibility calculations show that Leu183 is completely exposed. This results in a patch of hydrophobic surface juxtaposed to a positively charged region (Fig. 7), both of which are more pronounced than compared to human TIM. This hydrophobic region is close to the active site (less than 12 Å to Glu165) and hence might be a potential site for the specific inhibition of PfTIM by designed, hydrophobic, anionic molecules. It is noteworthy that the interaction of anionic dyes, like suramin, have been considered in the inhibition of trypanosomal TIM [25,26]. The enhanced hydrophobicity of this segment of the PfTIM surface may also be relevant in facilitating membrane attachment, a feature that appears important for parasitic glycolytic enzymes. Indeed, specific interaction of *P. falciparum* aldolase with band 3 of erythrocytes has been established [27].

Cysteine residues

PfTIM has four cysteine residues per monomer, amongst them Cys126 is conserved in all the species. One of the other cysteine residues occurs at the intersubunit interface (Cys13) and is probably important for dimerization; this residue is replaced by methionine in human TIM. The electron-density map of PfTIM shows additional density at hydrogen-bonding distance from the sulfur atom of Cys13. Extraneous density observed near cysteine residues has often been interpreted as molecules of reducing agent (such as dithiothreitol [DTT] or β-mercaptoethanol, present in the crystallization medium and forming mixed disulfides with the cysteine residues [28]) or as sulfenic acids [29,30]. This density, however, is not sufficient for a DTT molecule (the reducing agent used in the crystallization medium). The S–O distance of 3.25 Å also precludes sulfenic acid formation. Hence, this density has been assigned to a water molecule.

Tryptophan residues

Only two tryptophan residues occur in each subunit of PfTIM. Hence, tryptophan fluorescence studies on PfTIM are not complicated by spectral overlaps and provide a valuable means to monitor structural perturbations. Studies carried out on the unfolding of PfTIM

Figure 7

Comparison of the charge distribution on the surface of (a) PfTIM and (b) human TIM around residue Leu183. The residues Leu183 and Glu165 (in PfTIM) and Glu183 and Glu165 (in human TIM) are labeled. Red and blue represent negatively and positively charged regions, respectively, on the protein surface. (The figure was made using the program GRASP [52].)

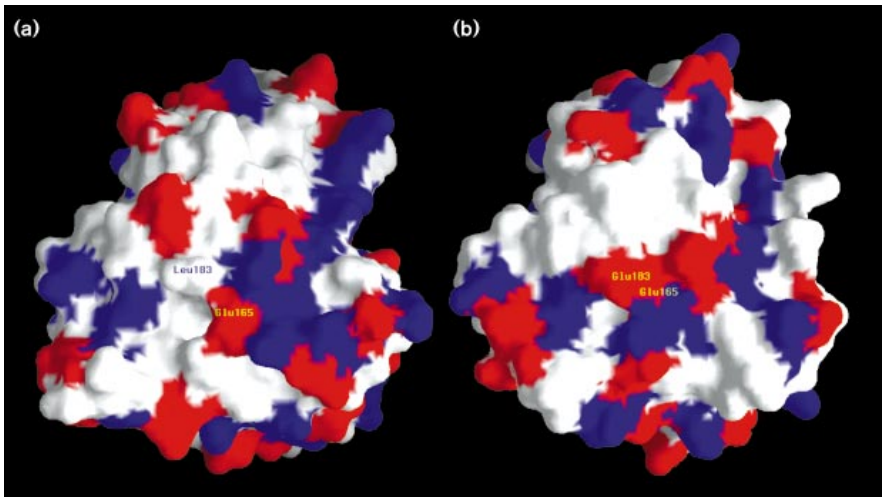

(RSG, SSR, HB and PB, unpublished data) show that chain unfolding precedes dimer dissociation. It is further observed that the protein unfolds at a much higher urea concentration when compared to human TIM. This is in agreement with our structural results, which suggest that the dimeric interface of PfTIM is apparently more apolar than the interface in the human TIM. Interestingly, apolar interactions at protein–protein surfaces have been shown to be thermodynamically dominant, a feature dramatically illustrated (using alanine scanning mutagenesis) in a study of the human growth hormone–receptor complex [31]. Furthermore, the interior of the β barrel in PfTIM is packed with bulkier and more hydrophobic residues when compared to that of human TIM, presumably contributing to the overall stability of the monomer.

Implications for drug design

The highly conserved nature of TIM sequences, in particular the active-site residues, makes it a difficult to design inhibitors specific to the parasite enzyme. Strategies of drug design in the context of the TIM structure have been considered previously with the trypanosomal enzyme. Wierenga *et al.* [15] and Lolis *et al.* [32] have drawn attention to residues required for catalysis as well as dimer assembly [15,32]. Inhibitors of TIM must be very effective as TIM has a high specific activity. Furthermore, TIM deficiency is known to cause severe disease in humans [21], requiring that the designed inhibitor must be highly specific for the parasite enzyme. Examination of the residues close to the active site that are not conserved between the human and parasite TIMs suggests that Phe96 and Cys13 might be plausible sites for differential attack by chemical reagents. The presence of a bulky, hydrophobic, aromatic residue like phenylalanine at position 96 in the parasite enzyme holds promise for the design of small molecule inhibitors, which could specifically interact with this residue via hydrophobic or stacking interactions. Such an approach has been shown to be effective in the case of thymidylate synthase inhibition [33]. In human TIM, residue 14 at the dimer interface is a methionine; in PfTIM the structurally equivalent residue (13) is a cysteine. Replacement of the equivalent Met14 in the human enzyme by glutamine has been shown to result in reduced stability of the dimer [20]. It has been found that modification of cysteine residues by iodoacetic acid in PfTIM results in the irreversible precipitation of the protein. The Asn71 sidechain carboxyamide group from the B monomer is positioned close to the sulfhydryl group of Cys13 of monomer A. It is known that, in the case of the chicken enzyme, this asparagine is susceptible to deamidation at pH8.0 [34]: the deamidation introduces a negative charge at the interface. Modification of Cys13 in PfTIM by iodoacetate leads to severe destablization of the labeled protein resulting in precipitation. In contrast, Cys13 in the engineered mutant Tyr74→Cys is locked into a disulfide bridge with Cys74 on the neighboring subunit. The disulfide bridged mutant protein is not precipitated by treatment with iodoacetic acid (RSG, SSR, HB and PB, unpublished data). Interestingly, species specific inhibition of TIM using the interface cysteine residue has been suggested [35].

A further important difference between the human and parasite TIMs is the replacement of a charged surface residue in the former (Glu183) with a hydrophobic residue in the latter (Leu183). The hydrophobic residue in PfTIM may play a role in membrane attachment within the erythrocyte. A significant body of evidence suggests the importance of the interaction of glycolytic enzyme with the erythrocyte cytoskeleton [6], a factor which may be particularly important for the malarial parasite. Specific inhibition of membrane attachment may provide an alternative strategy for interference with the normal physiology of the parasite resident in the erythrocyte host.

Biological implications

Triosephosphate isomerase (TIM) is an important house keeping enzyme found in almost every organism [32]. In recent years, there has been a renewed interest in the glycolytic enzymes from protozoan parasites, as these parasites seem to have a strong dependence on the glycolytic pathway for energy [26]. Among the various diseases that affect the tropical world one of the most severe is malaria. *Plasmodium falciparum,* the most prevalent malarial parasite in the Asian subtropical zone, is responsible for malignant subtertian malaria. The emergence of drug resistant strains of *P. falciparum* poses a new threat and demands the design of alternative drugs. There are no effective vaccines against malaria due to the elusive nature of the parasite, which escapes the immune system by spending part of its life cycle inside the red blood cell and by modifying its surface antigens periodically [36].

The unique biochemistry of the parasite offers prospects for drug design based on a comparative analysis of the glycolytic enzymes from humans and *P. falciparum*. In a recent report, it has been shown that during *P. falciparum* infection patients mount an antibody response to TIM [5], which may become membrane bound. Indeed another glycolytic enzyme, aldolase from *P. falciparum,* was found to elicit an immune response in monkeys and act as a protective antigen [37]. Increased localization of TIM has been shown to occur in several familial erythroenzymopathies [38]. In the case of schistosomal infection, TIM has been found localized on the membrane surface and acts as an antigen [6]. The crystal structure of *P. falciparum* TIM (PfTIM) opens fresh avenues for therapeutic drug design. A detailed comparison of the PfTIM structure to that of human TIM reveals that although the structures are substantially similar, subtle differences exist which may be exploited

in the design of specific inhibitors of enzyme activity and assembly. Two key differences have been identified which are of importance in such design: a significant difference in the surface hydrophobicity at residue 183; and differences in the residues Cys13 and Phe96 (which are methionine and serine, respectively, in human TIM). All these residues are close to the active site of the enzyme. The structural differences associated with these sites might be of importance for the preferential inhibition of PfTIM.

Materials and methods

Purification of PfTIM

The PfTIM gene was cloned into the expression vector pTrc 99A and called pARC1008 [7]. The protein was overexpressed in the *E. coli* strain AA200, which has a null mutation in the host TIM gene [39]. The clone was obtained from Astra Research Center, Bangalore, India. Expression of the TIM gene was under the control of the *trc* promoter inducible by isopropyl-β-D-thiogalactoside (IPTG). There was no significant leaky expression in the uninduced state. The conditions for overexpression were determined by varying the concentration of the inducer, the time of induction and the growth after induction. An overnight seed culture (5%) was used as inoculum for 500 ml of terrific broth [40]. 50 μg ml^{-1} of ampicillin were added to the medium for selection. The inoculated flasks were incubated on a shaker (250 rpm, 37°C) for 4 h. After induction with 0.8 M IPTG, the culture was further grown for 16 h. Cells were harvested by centrifugation in a Sorvall RC-5B centrifuge using a GS3 rotor at 4000 rpm for 10 min at 4°C. The harvested cells were resuspended in 20 ml of 100 mM Tris-HCl pH 8.0, 1 mM EDTA and lysed using a French press at 3000 psi in two cycles. Cell debris was discarded by centrifugation at 12 000 rpm for 30 min in a Sorvall SS34 rotor. The supernatant was diluted to 100 ml with ice cold water. The supernatant was raised to 70% (v/v) saturation in ammonium sulfate at 4°C. After 6 h storage at the same temperature, the precipitate was discarded by centrifugation at 12 000 rpm for 30 min at 4°C. The supernatant was subjected to further precipitation by 95% saturated ammonium sulfate at 4°C. The precipitate was collected by centrifugation and dissolved in 5 ml of cold water. This was extensively dialyzed against 20 mM Tris-HCl pH 8.0. The protein was further purified on an anion exchange column, Mono Q (10/10) using a Pharmacia FPLC system. The protein was eluted using a gradient of 0–0.5 M NaCl over a period of 50 min. The fractions containing TIM were identified by analysis using SDS polyacrylamide gel electrophoresis. The TIM containing fractions were pooled and dialyzed against cold water and lyophilized. The protein samples retained activity for several months upon storage at –20°C.

Crystallization of PfTIM

Crystals were grown at 23°C using the hanging-drop method. The reservoir solution contained 24% (w/v) PEG 6000 in HEPES buffer pH 7.5 containing 1 mM DTT. An 8 μl drop containing equal volumes of the reservoir and protein solutions (20 mg ml^{-1} in water) in the hanging drop placed on a presiliconized cover slip was equilibrated with the reservoir solution. The crystal grew over a period of two to six weeks to a size of $0.1\times0.5\times0.1$ mm. The crystals belong to monoclinic space group C2 with cell dimensions a = 98.91 Å, b = 47.64 Å, c = 118.43 Å, β = 108.26 Å. The asymmetric unit of the crystal is compatible with one dimer (Matthews coefficient 2.55 Å^3 Da^{-1} assuming a molecular weight of 26 kDa per monomer).

Data collection

Complete three-dimensional X-ray diffraction data were collected using a MAR imaging plate detector system mounted on a Rigaku RU200 X-ray generator operating at 40 kV, 60 mA. The details of the completeness and quality of the data is illustrated in Table 2. The crystals diffracted to 2.2 Å resolution. The data were processed with the DENZO suite of programs [41,42]. Reflection intensities were obtained by profile fitting. Radiation damage resulted in about 20% reduction in reflection intensities at the end of the data collection.

Structure solution

The structure was solved using molecular replacement techniques. Trypanosomal TIM, which shares 42.3% sequence identity with PfTIM, was used as the starting model. The coordinates of the trypanosomal enzyme were obtained from the Brookhaven National Laboratory Protein Data Bank [43] (code 5TIM). The rotation and translation functions were calculated using the program AMoRe [11]. Initial computations were performed using the coordinates of the trypanosomal dimer. The highest peak in the rotation function had a value of 17 while the very next peak, unrelated to the largest peak by the monoclinic symmetry or the noncrystallographic twofold axis pertaining to the dimer of PfTIM, was less than seven. This orientation also corresponded to the highest peak obtained in translation searches. The largest correlation coefficient in the translation function search was 46.5 compared to the next peak at 32.5. Examination of the protein packing corresponding to this solution revealed good intermolecular crystal contacts without any severe interpenetration.

Model building and refinement

The coordinates of trypanosomal TIM, suitably transformed to the PfTIM cell, were used for computing structure factors using the program X-PLOR [44]. The R factor between the computed and observed structure-factor amplitudes was 49.8% to a resolution of 3 Å. Initially the dimeric trypanosomal TIM as a whole and subsequently the individual A and B subunits of trypanosomal TIM were subjected to rigid-body refinement using data in the resolution shell 10–3 Å; the R factor reduced to 48.7%. A $2F_o–F_c$ map computed after rigid-body refinement was easy to interpret in terms of the amino acid replacements between trypanosomal TIM and PfTIM. An atomic model of PfTIM consistent with the amino acid sequence deduced from the gene sequence was constructed using the interactive graphics program O [45]. The loop 6 (residues 165–178) of the B subunit in

Table 2

Summary of data statistics and refinement statistics.

Total number of reflections measured	39 357
Redundancy	3.4
Total number of unique reflections	25 936
Number of unique reflections (resolution range 10–2.2 Å) $I/\sigma(I) > 2.0$	24 507
Completeness (resolution range 10–2.2 Å) $I/\sigma(I) > 2.0$ (%)	92.0
Completeness (last resolution shell 2.3–2.2 Å) $I/\sigma(I) > 2.0$ (%)	83.9
R_{merge} (resolution shell 2.28–2.20) (%)*	25.2
R_{merge} (%)*	8.9
Initial R factor (%)†‡	49.8
Initial free R factor (%)†‡	50.68
Final R factor $I/\sigma(I) > 2.0$ (resolution range 10–2.2 Å) (%)	19.8
Final free R factor $I/\sigma(I) > 2.0$ (resolution range 10–2.2 Å) (%)	25.4
Number of nonhydrogen atoms in the model	4085
Rms deviation in bond angles (°)	1.39
Rms deviation in bond lengths (Å)	0.007

*$R_{merge} = \Sigma|F_o - kF_c| / \Sigma F_o \times 100$. †R factor $= \Sigma|\langle I\rangle - I_h| / \Sigma\langle I\rangle \times 100$, where I_h is the intensity of a measurement and $\langle I\rangle$ is the average of the measurements for reflection h. ‡Values for the trypanosomal TIM model in the PfTIM cell.

PfTIM is in the open conformation, while it is almost closed in the model. An omit map corresponding to this region could be clearly interpreted in terms of the sequence of this segment in the open conformation. The two monomers of the initial model were refined independently. Each round of refinement consisted of positional refinement with repulsive potential, followed by simulated annealing from 2500°C and overall B-factor refinement or individual B-factor refinement at latter stages. 10% of the reflections, not included in the refinement, were used for the computation of the free R factor. Each stage of refinement was continued until the free R factor converged. Rounds of refinement were interspersed by manual map fitting. The initial four rounds of refinement were performed using data in the 10–3 Å resolution shell while for latter refinements, data in the 10–2.2 Å shell were used. When the free R factor was 29%, probable water molecules bound to the protein were located in $2F_o–F_c$ maps. A total of 171 water molecules were added to the model in three stages. At the current stage of refinement the model along with the water molecules (total of 4085 nonhydrogen atoms) has an R factor of 19.8% for 85% of the data between 10–2.2 Å. The free R factor calculated using the remaining 10% of the data within this resolution shell is 25.4%. The rms deviations of the bond length and angles from standard values are 0.007 Å and 1.39°, respectively. Table 2 shows the final refinement statistics for the PfTIM model.

Accession numbers

The coordinates and structure factors have been deposited in the PDB with accession codes 1YDV and R1YDVSF, respectively. The coordinates are available from the authors on request.

Acknowledgements

We are grateful to the Astra Research Centre, India for permission to use the cloned PfTIM gene. We thank RK Wierenga, MK Mathew and SC Mande for help at various stages of the project. We acknowledge the facilities provided by The Molecular and Cell Biology department, The Bioinformatics Centre, The Department of Biotechnology-supported Interactive Graphics facility and The Supercomputer Education and Research Centre at IISc. We thank Govindaswamy, James, Babu and Beena for technical assistance. SSV and RSG were supported by the University Grants Commision and the Council of Scientific and Industrial Research, India, respectively. The project was funded by grants from the Council of Scientific and Industrial Research, India.

References

1. Sherman, I.W. (1979). Biochemistry of *Plasmodium* (malarial parasites). *Microbiol. Rev.* **43**, 453–495.
2. Roth, E., *et al.*, & Rosa, R. (1988). The use of enzymopathic human red cells in study of malarial parasite glucose metabolism. *Blood* **71**, 1408–1413.
3. Orosz, F. & Ovadi, J. (1986). Dynamic interactions of enzymes involved in triosephosphate metabolism. *Eur. J. Biochem.* **160**, 615–619.
4. Knowles, J.R. (1991). Enzyme catalysis: not different, just better. *Nature* **350**, 121–124.
5. Ritter, K., Kuhlencord, A., Thomssen, R. & Bommer, W. (1993). Prolonged hemolytic anemia in malaria and autoantibodies against triosephosphate isomerase. *Lancet* **342**, 1333–1334.
6. Harn, D.A., Gu, W., Oligono, D.L., Mitsuyama, M., Gebremichael, A. & Ritcher, D. (1992). A protective monoclonal antibody specifically recognizes and alters the catalytic activity of triosephosphate isomerase. *J. Immunol.* **148**, 562–571.
7. Ranie, J., Kumar, V.P. & Balaram, H. (1993). Cloning of the triosephosphate isomerase gene of *Plasmodium falciparum* and expression in *Escherichia coli. Mol. Biochem. Parasitol.* **61**, 159–170.
8. Dobeli, H., Itin, C., Meier, B. & Certa, U. (1991). Is *Plasmodium falciparum* aldolase useful for rational drug design? *Acta Leiden* **60**, 135–140.
9. Dunn, C.R., *et al.*, & Holbrook, J.J. (1996). The structure of lactate dehydrogenase from *Plasmodium falciparum* reveals a new target for anti-malarial design. *Nat. Struct. Biol.* **3**, 912–915.
10. Reardon, D. & Farber, G.K. (1995). The structure and evolution of α/β barrel proteins. *FASEB J.* **9**, 497–503.
11. Navaza, J. (1994). AMoRe: an automated package for molecular replacement. *Acta Cryst. A* **50**, 157–163.
12. Sampson, N.S. & Knowles, J.R. (1992). Segmental movement: definition of the structural requirement for loop closure in catalysis by triosephosphate isomerase. *Biochemistry* **31**, 8482–8487.
13. Noble, M.E.M, Zeelen, J. Ph. & Wierenga, R.K. (1993). Structure of the 'open' and 'closed' state of trypanosomal triosephosphate isomerase, as observed in a new crystal form: implications for the reaction mechanism. *Proteins* **16**, 311–326.
14. Parker, J., Johnston, T.C., Borgia, P.T., Holtz, G., Remaut, E. & Fiers, W. (1983). Codon usage and mistranslation. *In vivo* basal level misreading of the MS2 coat protein message. *J. Biol. Chem.* **258**, 10007–10012.
15. Wierenga, R.K., Noble, M.E.M., Vriend, G., Nauche, S. & Hol, W.G.J. (1991). Refined 1.83 Å structure of trypanosomal triosephosphate isomerase crystallized in the presence of 2.4 M ammonium sulphate. *J. Mol. Biol.* **220**, 995–1015.
16. Ramachandran, G.N. & Sasisekharan, V. (1968). Conformation of polypeptides and proteins. *Adv. Protein Chem.* **23**, 283–438.
17. Lackowicz, J.R. (1983). *Principles of Fluorescence Spectroscopy*. Plenum press, NY, USA.
18. Noble, M.E.M, Zeelen, J.Ph. & Wierenga, R.K. (1993). Structure of triosephosphate isomerase from *E. coli* determined at 2.6 Å resolution. *Acta Cryst. D* **49**, 403–417.
19. Delboni, L.F., *et al.*, & Hol, W.G.J. (1995). Crystal structure of recombinant triosephosphate isomerase from *Bacillus stearothermophilus*. An analysis of potential thermostability factors in six isomerases with known three-dimensional structures points to the importance of hydrophobic interaction. *Protein Sci.* **4**, 2594–2604.
20. Mande, S.C., Mainfroid, V., Kalk, K.H., Goraj, K., Martial, J.A. & Hol, W.G.J. (1994). Crystal structure of recombinant human triosephosphate isomerase at 2.8 Å resolution. Triosephosphate isomerase related human genetic disorders and comparison with the trypanosomal enzyme. *Protein Sci.* **3**, 810–821.
21. Mainfroid, V., *et al.*, & Goraj, K. (1996). Three hTIM mutants that provide new insights on why TIM is a dimer. *J. Mol. Biol.* **257**, 441–456.
22. Wierenga, R.K., Borchert, T.V. & Noble, M.E.M. (1992). Crystallographic binding studies with triosephosphate isomerase: conformational changes induced by substrate and substrate-analogues. *FEBS Lett.* **307**, 34–39.
23. Williams, J.C. & McDermott, A.E. (1995). Dynamics of the flexible loop of triosephosphate isomerase: the loop motion is not ligand gated. *Biochemistry* **34**, 8309–8319.
24. Verlinde, C.L.M.J., *et al.*, & Opperdoes, F.R. (1992). Structure of the complex between triosephosphate isomerase and *N*-hydroxy-4-phosphono-butanamide: binding at the active site despite an 'open' flexible loop. *Protein Sci.* **1**, 1578–1584.
25. Wierenga, R.K., *et al.*, & Hol, W.G.J. (1987). Common elements on the surface of glycolytic enzymes from *Trypanosoma brucei* may serve as topogenic signals for import into glycosomes. *EMBO J.* **6**, 215–221.
26. Verlinde, C.L.M.J., *et al.*, & Hol, W.G.J. (1994). Protein crystallography and infectious diseases. *Protein Sci.* **3**, 1670–1686.
27. Dobeli, H., *et al.*, & Certa U. (1990). Expression, purification, biochemical characterization and inhibition of recombinant *Plasmodium falciparum* aldolase. *Mol. Biochem. Parasitol.* **41**, 259–268.
28. Silva, A.M., Cachau, R.E., Sham, H.L. & Erickson, J.W. (1996). Inhibition and catalytic mechanism of HIV-1 aspartic protease. *J. Mol. Biol.* **255**, 321–346.
29. Allison, W.S. (1976). Formation and reaction of sulfenic acids in proteins. *Accounts Chem. Res.* **9**, 293–299.
30. Mande, S.S., Parsonage, D., Claiborne, A. & Hol, W.G.J. (1995). Crystallographic analysis of NADH peroxidase Cys42Ala and Cys42Ser mutants: active site structures, mechanistic implications, and an unusual environment of Arg303. *Biochemistry* **34**, 6985–6992.
31. Wells, J.A. (1996). Binding in the growth hormone receptor complex. *Proc. Natl. Acad. Sci. USA* **93**, 1–6.
32. Lolis, E., Albert, T., Davenport, R.C., Rose, D., Hartman, F.C. & Petsko, G.A. (1990). Structure of yeast triosephosphate isomerase at 1.9 Å resolution. *Biochemistry* **29**, 6609–6618.
33. Jones, T.R. *et al.*, & Morse, C.A (1996). Structure based design of lipophillic quinazoline inhibitors of thymidylate synthase. *J. Med. Chem.* **39** 904–917.
34. Garza-Ramos, G., Perez-Monfort, R., Rojo-Dominguewz, A., de Gomez-Puyou, M.T. (1996). Species-specific inhibition of homologous enzymes by modification of nonconserved amino acid residues. The cysteine residues of the triosephosphate isomerase. *Eur. J. Biochem.* **241**, 144–120.

35. Sun, A.Q., Yuksel, K.U. & Gracy, R.W. (1992). Relationship between the catalytic center and the primary degradation site of triosephosphate isomerase: effects of active site modification and deamidation. *Arch. Biochem. Biophys.* 293, 382–390.
36. Su, X., *et al*., & Wellems, T.E. (1995). The large diverse gene family *var* encodes proteins involved in cytoadherence and antigenic variation of *Plasmodium falciparum*-infected erythrocyte. *Cell* 82, 89–100.
37. Certa, U., *et al*., & Perrin, L.R. (1988). Aldolase activity of a *Plasmodium falciparum* protein with protective properties. *Science* 240, 1036–1040.
38. Hollan, S., *et al*., & Farkas, T. (1995). Erythrocyte lipids in triosephosphate isomerase deficiency. *Proc. Natl. Acad. Sci. USA* 92, 268–271.
39. Anderson, A. & Cooper, R.A. (1970). Genetic mapping of a locus of triosephosphate isomerase on the locus of *E. coli* K12. *J. Gen. Microbiol.* 62, 329–334.
40. Sambrook, J., Fritsch, E.F. & Maniatis, T. (1989). *Molecular Cloning: a Laboratory Manual*. Cold Spring Harbor press, USA.
41. Otwinowski, Z. (1993). Oscillation data reduction program. In *Proceedings of the CCP4 study weekend: Data Collection and Processing*. (Sawyer, L., Isaacs, N. & Bailey, S., eds), pp. 56–62, SERC Daresbury Laboratory, Warrington, UK.
42. Minor, W. (1993). XDISPLAYF Program. Purdue University.
43. Berstein, F.C., *et al*., & Tasumi, M. (1977). The protein data bank: a computer-based archival file for macromolecular structures. *J. Mol. Biol.* 112, 535–542.
44. Brünger, A.T. (1992). *X-PLOR Manual, Version 3.1*. Yale University, New Haven, CT, USA.
45. Jones, T.A., Zou, J.Y., Cowman, S.W. & Kjeldgaard, M. (1991). Improved methods for building models in electron-density maps and the location of errors in these models. *Acta Cryst. A* 47, 110–119.
46. Olafsson, P., Matile, H. & Certa, U. (1992). Molecular analysis of *Plasmodium falciparum* hexokinase. *Mol. Biochem. Parasitol.* 56, 89–101.
47. Srivastava, I.K., Schmidt, M., Grall, H., Certa, U., Garcia, A.M. & Perrin, L.H. (1992). Identification and purification of glucose phosphate isomerase of *Plasmodium falciparum. Mol. Biochem. Parasitol.* 54, 153–163.
48. Hicks, K.E., Read, M., Holloway, S.P., Sims, P.F. & Hydwe, J.E. (1991). Glycolytic pathway of the human malaria parasite *Plasmodium falciparum*: primary sequence analysis of the gene encoding 3-phosphoglycerate kinase and chromosomal mapping studies. *Gene* 100, 123–129.
49. Read, M., Hicks, K.E., Sims, P.F. & Hyde, J.E. (1994). Molecular characterization of the enolase gene from malaria parasite *Plasmodium falciparum.* Evidence for ancestry within a photosynthetic lineage. *Eur. J. Biochem.* 220, 513–520.
50. Laskowski, R.A., MacArthur, M.W., Moss, D.S. & Thornton, J.M. (1993). PROCHECK: a program to check the stereochemical quality of protein structures. *J. Appl. Cryst.* 26, 283–291.
51. INSIGHTII (1993). Insight II user guide. Biosym Technologies, San Diego, CA, USA.
52. Nicholls, A., Bharadwaj, R. & Honig, B. (1993). GRASP: a graphical representation and analysis of surface properties. *Biophys. J.* 64, 166.